THE JOURNAL OF PHYSICAL CHEMISTRY B

Article

pubs.acs.org/JPCB

# Non-Gaussian Statistics and Nanosecond Dynamics of Electrostatic Fluctuations Affecting Optical Transitions in Proteins

Daniel R. Martin and Dmitry V. Matyushov*

Center for Biological Physics, Arizona State University, PO Box 871504, Tempe, Arizona 85287-1504, United States

Supporting Information

**ABSTRACT:** We show that electrostatic fluctuations of the protein−water interface are globally non-Gaussian. The electrostatic component of the optical transition energy (energy gap) in a hydrated green fluorescent protein is studied here by classical molecular dynamics simulations. The distribution of the energy gap displays a high excess in the breadth of electrostatic fluctuations over the prediction of the Gaussian statistics. The energy gap dynamics include a nanosecond component. When simulations are repeated with frozen protein motions, the statistics shifts to the expectations of linear response and the slow dynamics disappear. We therefore suggest that both the non-Gaussian statistics and the nanosecond dynamics originate largely from global, low-frequency motions of the protein coupled to the interfacial water. The non-Gaussian statistics can be experimentally verified from the temperature dependence of the first two spectral moments measured at constant-volume conditions. Simulations at different temperatures are consistent with other indicators of the non-Gaussian statistics. In particular, the high-temperature part of the energy gap variance (second spectral moment) scales linearly with temperature and extrapolates to zero at a temperature characteristic of the protein glass transition. This result, violating the classical limit of the fluctuation−dissipation theorem, leads to a non-Boltzmann statistics of the energy gap and corresponding non-Arrhenius kinetics of radiationless electronic transitions, empirically described by the Vogel−Fulcher−Tammann law.

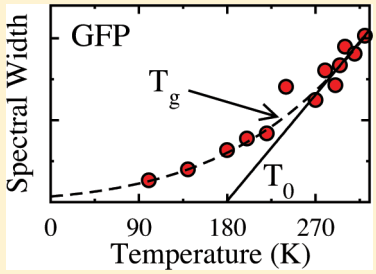


## INTRODUCTION

Electrostatics is significant for protein function and stability.[1−4] The electrostatic potential at the active site of an enzyme is a combination of contributions arising from the hydration water and the protein. The two subsystems are in fact strongly coupled. The energy of nonbonded (van der Waals and electrostatic) interactions of the protein atoms is significantly below the corresponding interaction energy between the protein and water (with the ratio of about 1:2[5]). The pull from the interfacial water, originating from the solvation free energy of the surface residues, allows proteins to maintain a flexible folded structure and, in the case of intrinsically disordered proteins, even to possess a heterogeneous ensemble of conformations close in energy.[6,7] When dried, proteins stiffen and their relaxation time rises by about 6 orders of magnitude.[8]

The protein−water system exhibits mutual influence. It is not only that water affects the protein, but the presence of a protein in solution dramatically alters the structure of the water shells surrounding it. The average interaction strength of hydration waters with the protein residues often exceeds the interaction strength between the waters themselves.[9] Water thus wets the protein, with a resulting enhanced density at the protein surface.[10] That surface is, however, highly heterogeneous.[11,12] A complex patchwork of polar and ionized residues is organized in surface clusters with charge complementarity, i.e., the opposite-charge residues are neighbors.[13,14] Given a typical size of the hydration layer, involving ∼300−500 waters in the first solvation shell only, a new type of thermal bath emerges. It might possess a fluctuation spectrum and dynamics quite distinct from those of small organic molecules or ions typically encountered in solution chemistry.[15] The fluctuation spectrum of the interfacial ensemble can be probed by optical chromophores placed either near the interface or inside the protein[16] or by electron transfer between cofactors inserted inside the protein.[17] The statistics of the protein−water interface can therefore produce properties not observed for a system with less extended hydration layers.

The traditional paradigm for describing the electrostatic response of a dense polar liquid goes back to Born[18] and Onsager[19] solvation models employing the linear response approximation, i.e., the assumption that the response of a solvent to a changing charge distribution of the solute is a linear function of that change.[20,21] This approximation is certainly correct for small perturbations of Hookean springs representing the medium: their small displacements are proportional to a small pulling force exerted by external charges. Since the force constant of a Hookean spring also defines the fluctuations of spring elongations under thermal agitation, the theory predicts a clear connection between the response of a medium to an external perturbation and thermal fluctuations in the absence of any perturbation. This connection is usually framed in terms of the fluctuation−dissipation theorem (FDT).[22] It is at this logical step, connecting averages to fluctuations, where the

**Received:** June 12, 2012
**Revised:** August 1, 2012
**Published:** August 3, 2012





dx.doi.org/10.1021/jp305757t | J. Phys. Chem. B 2012, 116, 10294−10300

medium of springs might become an inadequate representation of a hydrated protein.

It is now well appreciated that a folded protein does not reside in a single equilibrium well, but instead walks through a number of hierarchically organized conformational substates.[23−25] These complex activated motions result in a wide distribution of relaxation times. Moreover, hydration water interfacing the protein is organized in a patchwork of substates corresponding to the local polarity of the protein surface it faces.[12] The result is a complex landscape of states between which the corresponding water clusters can potentially fluctuate, either by thermal excitations or driven by vibrations and conformational motions of the protein.[26,27]

The broad spectrum of coupled protein−water motions reflects complexity and large configurational entropy of the protein−water system.[28−31] In terms of electrostatic observables, this complexity implies that electrostatic fluctuations might not necessarily be derived from the mechanical pulling force, but, to a greater extent, are driven by the availability of the configurational substates. In other words, the fluctuations of the protein−water electrostatic field and potential might be ruled more by the configurational entropy of the interface than by their enthalpic cost. The entropic signature in thermal fluctuations can be unraveled from the temperature dependence of the averages, the second spectral moment in particular. We show below that conformational entropy of the protein−water interface indeed causes deviations from the predictions of the FDT and, therefore, from the traditional connection between the averages and variances.

Consistent with unique properties of a large ensemble making the protein−water interface, we have recently found that the breadth of electrostatic fluctuations calculated from numerical simulations of redox proteins far exceeds the expectations of linear response based on the arguments of a medium of mechanical, linearly responding springs.[32] The simulations performed for half-redox reactions of redox-active proteins have pointed to a mechanism of entropy-driven fluctuations originating from the multitude of configurational substates. Here we extend this analysis to optical transitions in a green fluorescent protein (GFP). The advantage of this type of system over half redox reactions studied previously is that our proposal is directly accessible to spectroscopic experimental testing.

Wild-type GFPs show a complex excited-state photochemistry, with the excited-state proton-transfer reaction producing the dominantly fluorescent anionic form.[33] The relative population of neutral and anionic forms can be modified by mutation.[34] Here, following Vallverdu et al.,[35] we eliminate the complexity of the excited-state proton transfer by using the S65T mutant[36] (PDB entry 1EMA, Figure 1), where the serine residue at position 65 is replaced by a threonine. In this mutant, the chromophore exists only in the anionic form. Here we employ classical molecular dynamics (MD) simulations with the force field based on fixed atomic charges of the chromophore[35] to study the fundamental problem of the entropic driving force of interfacial fluctuations as projected on the statistics and dynamics of the optical energy gap.

## THERMODYNAMIC RELATIONS

The statistics of the nuclear modes affecting the energy gap $\Delta E$ between the ground and excited states of a chromophore is defined by singling out the energy gap "reaction coordinate" $X = \Delta E$ from the manifold of the nuclear degrees of freedom of the system.[21,37] This procedure defines the free energy surface along the reaction coordinate $X$

$$\exp[-\beta F_i(X)] \propto \langle \delta(X - \Delta E(Q)) \rangle_i \quad (1)$$

In this equation, $\Delta E(Q)$ depends on a manifold of nuclear degrees of freedom $Q$, the thermal motions of which are collectively projected on a single reaction coordinate $X$. Further, $\delta(x)$ is Dirac's delta-function and $\langle ... \rangle_i$ denotes the statistical ensemble average in either singlet-ground, $i = 0$ (S0), or singlet-excited, $i = 1$ (S1), state of an optical dye; $\beta = 1/(k_B T)$ is the inverse temperature.

The most probable value of the energy gap gives the minimum of the free energy surface $F_i(X)$, which we define as $\langle X \rangle_i$. At the same time, $\langle X \rangle_i$ is the average transition energy between the two electronic states (Figure 2). One can power expand the free energy $F_i(X)$ in small deviations $\delta X = X - \langle X \rangle_i$ from the minimum. The lowest-order expansion is quadratic

$$F_i(X) = F_{0i} + (X - \langle X \rangle_i)^2/(2\sigma_i^2) \quad (2)$$

Equation 2 represents a truncated, parabolic expansion of a generally nonparabolic free energy surface. A local quadratic expansion around the minimum $\langle X \rangle_i$ can always be done mathematically, regardless of whether the free energy $F_i(X)$ is globally parabolic or not. In that sense, $\sigma_i$ are just expansion coefficients. The coefficients $\sigma_i$ specify the curvatures of the free energy surfaces at the bottom; different $\sigma_i$ mean different curvatures (Figure 2).

In the case when the free energies $F_i(X)$ are globally quadratic, $\sigma_i^2$ loses its dependence on the state $i$ and becomes the variance of the statistical variable $X$, $\sigma_i^2 = \sigma^2 = \langle (\delta X)^2 \rangle$.[38] The existence of global expansion coefficients, independent of the electronic state, is a signature of the global non-Gaussian statistics of the electrostatic fluctuations, in contrast to an approximate local quadratic expansion around each minimum. A typical optical spectrum has its highest intensity around its maximum and, therefore, mostly reports on the statistics of electronic transitions near the bottom of the free energy surface. Accordingly, an optical band shape can often be fitted to a Gaussian function, which, however, does not imply global

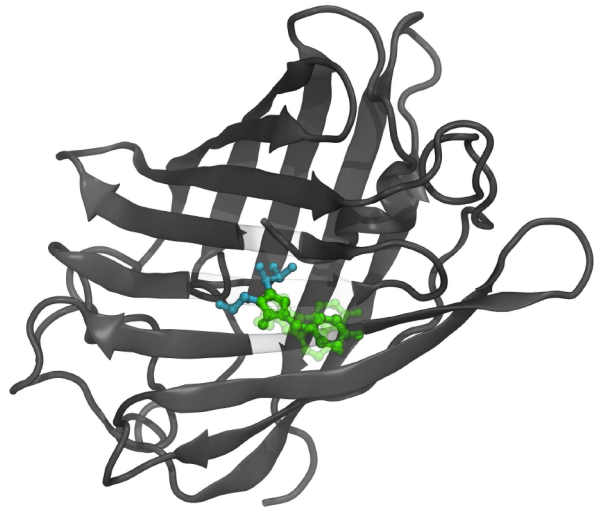

**Figure 1.** Cartoon of the green fluorescent protein (GFP) with the chromophore in the center (PDB 1EMA). Several conformations of the chromophore are superimposed in the image to stress on a high flexibility of the chromophore, resulting in non-Gaussian statistics of the electrostatic energy gap.

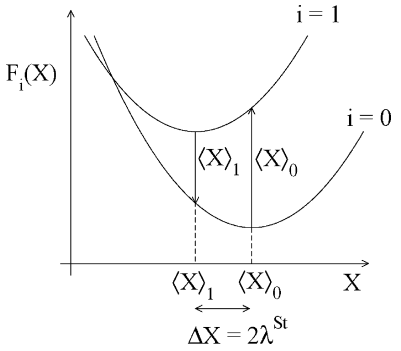


**Figure 2.** Schematic diagram of the free energy surfaces $F_i(X)$ at the configuration allowing two optical transitions, absorption and emission. The corresponding average transition energies are $\langle X\rangle_0$ (absorptions) and $\langle X\rangle_1$ (emission). The difference between either the vertical transition energies or the horizontal separation between the minima makes the Stokes shift $\Delta X$. The curvature of each free energy surface at its bottom determines $\sigma_i^2$ (eq 2).

Gaussian statistics of the medium fluctuations. Only when the fit of both the absorption and emission band shapes can be done with the same Gaussian width does this become a signature of globally Gaussian fluctuations of the thermal bath.

Yet another signature of global Gaussian statistics is the ability to predict the spectral widths from the difference between average transition energies $\langle X\rangle_i$, which is the Stokes shift. For globally Gaussian fluctuations, it is connected to the variance, i.e., the spectral width, as follows:[39,40] $\Delta X = |\langle X\rangle_1 - \langle X\rangle_0| = \beta\sigma^2$. This condition is not satisfied for nonparabolic free energy surfaces.[38] Therefore, the ratio of the second and first cumulants can be used to quantify the extent of deviation from the Gaussian statistics. The parameter characterizing the global statistics of the system is defined as follows

$$\chi_G = \beta\bar{\sigma}^2/\Delta X = \lambda^{\mathrm{var}}/\lambda^{\mathrm{St}} \tag{3}$$

where $\bar{\sigma}^2 = (\sigma_1^2 + \sigma_2^2)/2$ is the mean variance.

In order to establish a connection between the language of cumulants and corresponding spectral moments of optical transitions[38,39] to the language of reorganization energies used in theories of radiationless transitions and electron-transfer reactions,[20,21,41] we will represent the variance $\sigma_i^2$ and the Stokes shift $\Delta X$ in terms of two reorganization energies,[32] the Stokes-shift reorganization energy $\lambda^{\mathrm{St}} = \Delta X/2$ and the variance, or curvature, reorganization energy $\lambda_i^{\mathrm{var}} = \beta\sigma_i^2/2$. In the global Gaussian statistics of the energy-gap fluctuations, $\lambda_1^{\mathrm{var}} = \lambda_2^{\mathrm{var}} = \lambda^{\mathrm{St}}$. A deviation from either of these equalities indicates the breakdown of the Gaussian statistics. We find here that the first equality holds significantly better than the second, the deviation from it is quantified by $\chi_G$ (eq 3).

In addition to the global parameter $\chi_G$, one can also ask how nonparabolic each individual free energy surface is, i.e., how reliable is the local parabolic expansion when tested by the spectral moments. We will use the statistical coefficient of excess[37] for this purpose, quantifying the nonparabolic shape of each free energy surface

$$\chi_i = \langle(\delta X)^4\rangle_i/[3\langle(\delta X)^2\rangle_i^2] \tag{4}$$

Both $\chi_G$ and $\chi_i$ are equal to unity when the global free energy surfaces are reduced to parabolas and no higher terms in $\delta X$ appear in the series expansion in eq 2.

The temperature dependence of the average transition energy is another experimentally accessible observable quantifying deviations from the Gaussian statistics of the energy gap. The temperature derivative of $\langle X\rangle_i$ (thermochromic coefficient[42]) can be directly calculated from eq 1

$$s_i = -k_B^{-1}(\partial\langle X\rangle_i/\partial T)_V = -\beta^2\langle\delta X\delta E_i\rangle_i \tag{5}$$

where $E_i(X) = \partial(\beta F_i(X))/\partial\beta$ is the internal energy derived from the corresponding free energy surface (see the Supporting Information). When the quadratic expansion of eq 2 is used here, one gets for the thermochromic coefficient

$$s_i = -\frac{\beta\langle(\delta X)^3\rangle_i}{2\sigma_i^2}\left(\frac{\partial \ln \sigma_i^2}{\partial \ln T}\right)_V \tag{6}$$

The third cumulant $\langle(\delta X)^3\rangle_i$ is zero in the Gaussian limit, and so is the thermochromic coefficient. Therefore, Gaussian statistics excludes the possibility of constant-volume thermochromism. At constant pressure, the transition energy will be affected by the alteration of the density with temperature. The dependence of spectral moments on the solvent density is specific to a particular transition and requires modeling in each case (see Supporting Information). It can, however, be experimentally accounted for by combined changes of temperature and pressure.

The temperature dependence of the variance $\sigma_i(T)^2$ follows from the thermodynamic average with the free energy surface in each state, $\sigma_i^2 \propto \int\delta X^2 \exp[-\beta F_i(X)]\,dX$. If the Hookean enthalpy $H_i(X) \propto X^2$ dominates each free energy surface, the obvious result is the proportionality to temperature, $\sigma_i(T)^2 \propto T$. This is also the standard result of the classical limit of the FDT.[22] The difference of the problem at hand from the standard formulation of the FDT, involving adding a weak external perturbation to the system Hamiltonian, is that $X$ is a collective variable, absorbing many microscopic coordinates into it. The result is that both enthalpy and entropy contribute to $F_i(X) = H_i(X) - TS_i(X)$. If the entropy contribution is substantial, the temperature dependence of $\sigma_i^2$ is more complex. The limit of temperature-independent $\sigma_i^2$ corresponds to entropy domination in the free energy.

There are both microscopic considerations and numerical simulation data behind the notion that the high-temperature functionality of $\sigma_i(T)^2$ should be a linear function of temperature, $a + bT$, instead of a simple proportionality $\sigma_i(T)^2 \propto T(a=0)$ predicted by the FDT. Deviations from this prediction lead to a non-Boltzmann distribution of energy gaps and non-Arrhenius kinetics of radiationless transitions. Charge transfer in small molecules in polar liquids shows $a > 0$ in this relation.[38] The statistics of the protein−water interface is potentially more complex, and one might expect other scenarios. In fact, the results of numerical high-temperature simulations presented here produce $a < 0$. This finding implies $\sigma_i(T_0) = 0$. The temperature $T_0$ can be identified as the temperature of kinetic arrest[43] for radiationless transitions.[37] This limit is of course never reached, which requires a strong deviation of $\sigma_i(T)^2$ from the linear trend at a temperature $T_g \geq T_0$. As with the glass-transition temperature of a homogeneous glass former,[43] the crossover temperature $T_g$ depends on the observation window, which is the length of the simulation trajectory in numerical simulations.

## RESULTS

**Free Energy Surfaces and Non-Gaussian Statistics.** We calculate the Coulomb interaction of the chromophore built within the GFP's fold with the "solvent" composed of the protein, water, and dissolved ions (0.1 M). Since the difference of interaction energies is taken at each instantaneous nuclear configuration, $X$ is the Coulomb interaction energy of difference atomic charges $\Delta q_j$ between the ground and excited states of the chromophore with the atomic charges of the solvent. This is how the statistics and dynamics of this stochastic variable were calculated from MD trajectories. We start with the statistical distribution of $X$, leaving the technical details and simulation protocols to the Supporting Information.

Solid lines in Figure 3 refer to the free energy surfaces (eq 1) of the ground ($i$ = 0, S0) and excited ($i$ = 1, S1) states of the GFP's chromophore versus $X$. The most striking result of this analysis is the small separation between the minima, even though each simulation trajectory is produced with a different charge distribution of the chromophore. Consequently, the Stokes shift $\Delta X$, and the corresponding reorganization energy $\lambda^{St}$, are very small. The free energy surfaces are, however, broad and the reorganization energy $\lambda^{var}$, characterizing their curvature at the bottom, is significantly higher than $\lambda^{St}$. Consequently, the parameter $\chi_G$ describing the global statistics of electrostatic fluctuations (eq 3) is large (Table 1). Despite this global indication of the non-Gaussian statistics, each individual free energy surface is very close to a parabola, as indicated by parameters $\chi_i$ also listed in Table 1. The result of this analysis is that each individual surface is well described by a parabola, but one cannot extend the expectations of the Gaussian picture to both electronic states.

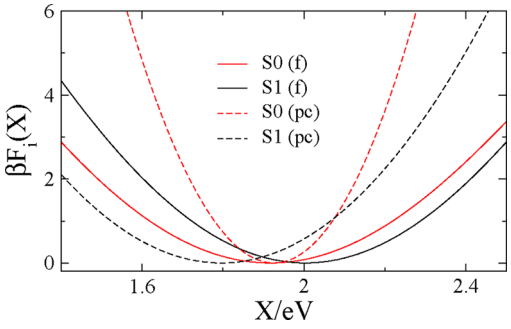


**Figure 3.** Free energy surfaces $\beta F_i(X)$ vs the energy gap coordinate $X$ for flexible (f) GFP protein in solution and the same solution with both the protein and the chromophore motions frozen (pc). The minima of the free energy curves are all shifted to the zero level.

**Table 1. Statistical Parameters Characterizing Free Energy Surfaces along the Energy Gap Reaction Coordinate**[a]

| state[b] | $\langle X\rangle_i$ | $\lambda_i^{var}$ | $\chi_i$ | $\chi_G$ |
|---|---|---|---|---|
| S0(f) | 1.93 | 0.92 | 1.11 | 25.17 |
| S1(f) | 2.00 | 0.84 | 1.03 | |
| S0(pc) | 1.93 | 0.20 | 1.00 | 6.25 |
| S1(pc) | 1.79 | 0.68 | 1.00 | |
| S0(p) | 1.97 | 0.27 | 1.04 | 11.50 |
| S1(p) | 1.88 | 0.76 | 1.01 | |
| S0(i) | 1.67 | 0.92 | 0.99 | 24.04 |
| S1(i) | 1.75 | 1.01 | 1.00 | |

[a]All energies are in eV. [b]States are denoted as follows: (f) flexible, all motions are allowed, (p) when the protein is rigid, (pc) when the protein and chromophore are rigid, and (i) when only ions are fixed. The rmsd of the center-of-mass of the chromophore relative to the center of mass of the protein drops from ~4 to ~0.1 Å upon freezing of the protein.

Several simulation protocols were designed to interrogate the origin of the non-Gaussian statistics. Motions of three components of the system, protein, chromophore, and ions, have been frozen in separate simulation runs. Allowing all components of the system to be flexible and move is the standard protocol labeled as "f" in Table 1. Freezing the protein motions while allowing chromophore's motions ("p" in Table 1) reduces $\chi_G$ by about a factor of 2. Further freezing of the chromophore's motions reduces $\chi_G$ by another factor of 2 ("pc" in Table 1). The reduction is largely a result of decreasing $\lambda_i^{var}$, as is clearly seen from increasing curvatures of the corresponding free energy surfaces shown by the dashed lines in Figure 3. However, $\lambda_0^{var}$ is reduced more dramatically than $\lambda_1^{var}$, opening a wide gap between the two variance reorganization energies not seen for a flexible protein. The origin of this effect is not clear.

In order to investigate a possible role of ions in producing the non-Gaussian statistics, a separate simulation was carried out by decreasing the number of ions to the minimum required to neutralize the simulation cell and fixing their coordinates during the subsequent simulation runs (marked as "i" in Table 1). While there is a noticeable effect of the ions' motion on the $\lambda$'s listed in Table 1, they clearly do not induce non-Gaussian electrostatic fluctuations.

These separate simulations clearly show that flexibility of the protein, and of the chromophore within the protein scaffold, are the main contributors to the observed separation between $\lambda^{St}$ and $\lambda^{var}$. However, even when both the protein and the chromophore are frozen, the energy gap produced by the hydration water is still non-Gaussian. While the origin of this effect is not entirely clear, it might be related to non-Gaussian electrostatic fluctuations[44] originating from flipping of domains of polarized water formed at surface residues of varying polarity.

**Nanosecond Dynamics of the Energy-Gap Fluctuations.** The dynamics of the energy gap fluctuations are traditionally represented by the Stokes shift time correlation function $C_i(t) = \langle \delta X(t)\delta X(0)\rangle_i$. Figure 4 shows the loss function

$$\chi''_i(\omega) = (\beta\omega/2)C_i(\omega) \tag{7}$$

where $C_i(\omega)$ is the Fourier transform of the function $C_i(t)$.

The loss function of the entire electrostatic energy gap $X$ displays two peaks typically found for the Stokes shift dynamics of hydrated proteins[27,45] (Figure 4a). While the existence of ~1 ps component in the loss spectrum of a chromophore in close proximity to water is generally expected, the appearance of a slow relaxation peak in the ~1−3 ns range is specific for hydration of large soft solutes[46] and for proteins in particular.[45]

The loss function $\chi''_i(\omega)$ conveniently separates the dynamics into separate relaxation components. It does not, however, provide a consistent view of their relative contributions to the reorganization energy given by the integral of the loss function scaled with the $\omega^{-1}$ factor

$$\lambda_i^{var} \propto \int_0^\infty \chi''_i(\omega)(d\omega/\omega) \tag{8}$$

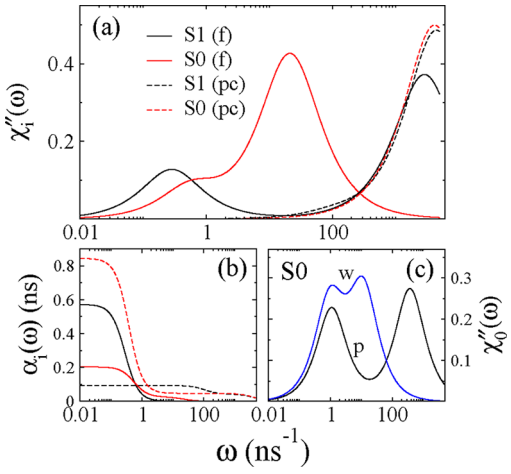


**Figure 4.** Normalized loss spectra $\chi''_i(\omega)/\chi'_i(0)$ of the energy gap fluctuations of the flexible and protein−chromophore frozen states (a). Panel (b) shows $\alpha_i(\omega) = \chi''_i(\omega)/(\omega\chi'_i(0))$; the results for the frozen protein−chromophore are multiplied by a factor of 300 to bring them to the scale of the plot. Panel (c) shows the water (w) and protein (p) components of $\chi''_i(\omega)/\chi'_i(0)$ in the ground (S0) state of the chromophore.

Therefore, Figure 4b shows the scaled function $\alpha_i(\omega) = \chi''_i(\omega)/(\omega\chi'_i(0))$, which also has the advantage of displaying the characteristic relaxation time at $\omega = 0$

$$\alpha_i(0) = \langle\tau\rangle_i, \quad \langle\tau\rangle_i = [C_i(0)]^{-1}\int_0^\infty C_i(t)\,dt \tag{9}$$

The origin of the slow Stokes-shift component is clarified by the simulations with the frozen protein motions. As is seen from Figure 4a, the slow relaxation peak completely disappears in that case. The Stokes-shift dynamics also become single exponential, with the dominant time of ≃0.2 ps characteristic of water relaxation (see Supporting Information). Therefore, the slow relaxation component is the dominant contributor to $\lambda_i^{var}$ (Figure 4b), and its disappearance is signaled by a significant decrease of the variance reorganization energy for frozen protein−chromophore configurations (Table 1).

The slow dynamics in the case of a flexible protein are not caused by the protein motions alone, but instead by the coupled motions of the protein and its hydration layer.[26,27] This is clearly seen in Figure 4c presenting the water and protein components of the Stokes-shift loss function. The high-frequency peak represents hydration waters slowed down by the contact with a large solute.[47,48] The lower-frequency peak traces the protein dynamics and can therefore be assigned to waters strongly bound to the protein surface and collectively following the protein motions.[49] An attempt to separate the hydration layer and the protein into two different subsystems requires assuming that the interactions within each subsystem are stronger than between the two. For water, strong binding to protein residues,[9] at least at parts of the surface, requires considering fluctuations of the protein−water interface as collective excitations.[26,50,51]

**Temperature Dependence.** The temperature dependence of the ground-state variance, $\sigma_0(T)^2$, is shown in Figure 5. In addition, the average electrostatic energy $\langle X\rangle_0(T)$ is given in the inset. Consistent with other indications of the non-Gaussian statistics of the electrostatic fluctuations, the constant-volume thermochromic coefficient is nonzero (see eq 6). The negative

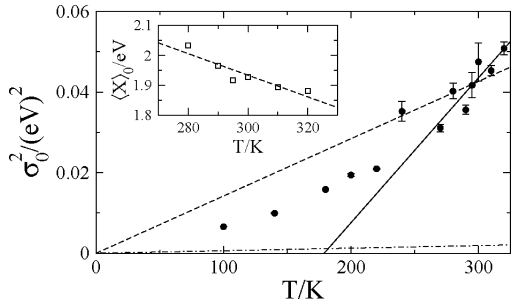


**Figure 5.** Temperature dependence of the variance of the donor−acceptor energy gap from NVT MD simulations in S0 state (points, error bars are equal to the point size at lower temperatures). The solid line is the linear fit of the high-temperature portion of the simulation data, and the dashed line is the fit of the same data to the FDT, crossing zero at $T = 0$. The dash-dotted line is the prediction of the linear response/FDT, $\sigma_0^2 = 2\lambda^{St}k_BT$ with $\lambda^{St}$ taken at 300 K. The inset shows the temperature dependence of the average ground−excited transition energy, $\langle X\rangle_0$. The dashed line in the inset is a liner fit through the simulation points.

linear slope of $\langle X\rangle_0$ is qualitatively consistent with experiment,[52] even though it was done at constant pressure.

The most interesting result is the behavior of $\sigma_0(T)^2$. Its temperature dependence turns out to be noticeably steeper than the prediction of the FDT (dashed line in Figure 5). This dependence implies that the reorganization energy $\lambda_0^{var}$ increases with increasing temperature, in contrast to the typically observed[38] temperature decrease of $\lambda^{St}$. The linear fit of the high-temperature portion of $\sigma_0(T)^2$ extrapolates to zero at $T_0 \simeq 180$ K, in the range of glass transition temperatures reported for partially hydrated protein powders.[53]

The identification of the temperature at which $\sigma_i(T)^2$ extrapolates to zero with the temperature of kinetic arrest naturally follows from the observation that the rate of radiationless transitions is proportional to the probability of reaching the point $X = 0$ at which electronic tunneling is allowed by Fermi's golden rule.[20,21,41] The rate of radiationless transitions $k_{NR}$ is then

$$k_{NR} \propto \exp[-(\langle X\rangle)^2/(2\sigma^2)] \propto \exp[-A/(T - T_0)] \tag{10}$$

Equation 10 predicts that the high-temperature portion of the radiationless (electron transfer) kinetics will be described by the Vogel−Fulcher−Tammann (VFT) temperature law, with the limiting temperature $T_0$ typically identified with the Kauzmann temperature of the ideal glass transition.[43] Derivation of eq 10 also presents a rare, and widely sought for,[43] case when the VFT dynamics can be consistently derived from thermodynamic arguments.

We stress here that the actual temperature variation of $\sigma_i(T)^2$ will not follow a linear dependence as drawn by the solid line in Figure 5, but will deviate from it at the point of glass transition when the collective (nanosecond at ≃300 K) motions of the interface become sufficiently slow to cross the experimental observation window.[54] Their kinetic arrest is expected at this glass-transition temperature $T_g > T_0$, with the restoration of the linear response $\sigma_i(T)^2 \simeq 2k_BT\lambda^{St}$ at the crossover (shown by the dash-dotted line in Figure 5). This qualitative picture seems to be followed by the low-temperature portion of $\sigma_0(T)^2$ from simulations (Figure 5), although with a slope higher than the estimate from $\lambda^{St}$ at 300 K. The difference is attributed to a finite trajectory length in simulations, similar to the effect of cooling rate in the laboratory glass transition.


dx.doi.org/10.1021/jp305757t | J. Phys. Chem. B 2012, 116, 10294−10300

## CONCLUDING REMARKS

We have found that electrostatic interactions of the GFP's chromophore with the protein−water solvent are characterized by both slow (nanosecond) dynamics and non-Gaussian statistics. Both properties are driven by the coupling of the soft vibrations of the protein to hydration water. The system returns to fast dynamics and nearly Gaussian statistics when the motions of the protein and chromophore are frozen.

The non-Gaussian electrostatics projects itself on the free energy surfaces $F_i(X)$, which do not satisfy the rules of global Gaussian statistics (equivalent to the linear response approximation[38]). In particular, the variance, or curvature, reorganization energy $\lambda_i^{\mathrm{var}}$ significantly exceeds the Stokes-shift reorganization energy $\lambda^{\mathrm{St}}$ calculated from the separation of the free energy minima (Figure 2). The origin of this effect is either the intrinsic nonparabolic shape of the free energy surfaces[40] or the fact that the observed $F_i(X)$ are nonergodic, referring only to the phase space accessible to statistical sampling on a finite observation time.[32] In the latter case, the fluctuations of a nonergodic nuclear mode (coupled protein−water motions) are resolved on the observation time (simulation or reaction time), but one of the two equilibrium states contributing to $\lambda^{\mathrm{St}}$ is not accessed on the observation time. In the case of electronic transitions in proteins, this inaccessible configuration is the equilibrium conformation in one (often excited) electronic state. This scenario leads to an excess of $\lambda_i^{\mathrm{var}}$ over $\lambda^{\mathrm{St}}$, at the same time favoring locally parabolic free energy surfaces.[55] This scenario is consistent with the present observations. Since MD, offering access to finite-time trajectories, does not allow a complete equilibrium sampling, our focus here is on observable consequences of this phenomenology, instead of its origin.

The fluctuation spectrum of the protein−water interface is strongly affected by the configurational entropy, competing with the enthalpy in the overall cost of producing a fluctuation. A number of observables are predicted to report on this effect. In particular, the constant-volume temperature dependence of the average energy gap (optical transition energy) and the energy gap variance (inhomogeneous broadening) are shown to deviate from the predictions of the Gaussian statistics and the fluctuation−dissipation theorem. These observations translate to the kinetics of radiationless transitions and/or protein electron transfer.

The temperature dependence of the rate of electron transfer is predicted to follow the VFT law, typically found in fragile glass formers.[43] The VFT dynamics of near-equilibrium fluctuations studied here might be a precursor of even stronger non-Arrhenius kinetics found when the protein starts to unfold.[56] From the thermodynamic viewpoint, a large $\chi_G$ strongly reduces the amount of energy dissipated into the heat when the electron is transferred in biological energy chains.[32] There is therefore a strong preference, and evolutionary pressure, for $\chi_G \gg 1$ in energy chains of biology required to battle the conflicting requirements of low energy input and a large number of electron hops.[57] The large $\chi_G$ observed here is therefore predicted to be broadly present in redox proteins participating in electron transport chains. Indeed, $\chi_G > 1$ has recently been reported for an optical transition in a metal-free cytochrome *c*.[58]

## ASSOCIATED CONTENT

### Supporting Information

Description of the simulation protocol and multiexponential fits of time correlation functions. This material is available free of charge via the Internet at http://pubs.acs.org.

## AUTHOR INFORMATION

### Corresponding Author

*E-mail: dmitrym@asu.edu.

### Notes

The authors declare no competing financial interest.

## ACKNOWLEDGMENTS

This research was supported by the National Science Foundation (CHE-1213288). CPU time was provided by the National Science Foundation through TeraGrid resources (TG-MCB080116N). We are grateful to Dor Ben-Amotz for helpful comments on the manuscript.

## REFERENCES

(1) Dill, K. A. *Biochemistry* **1990**, *29*, 7133−7155.
(2) Warshel, A.; Sharma, P. K.; Kato, M.; Parson, W. W. *Biochim. Biophys. Acta* **2006**, *1764*, 1647−1676.
(3) Cheung, M. S.; García, A. E.; Onuchic, J. *Proc. Natl. Acad. Sci. U.S.A.* **2002**, *99*, 685−690.
(4) Papoian, G. A.; Ulander, J.; Eastwood, M. P.; Luthey-Schulten, Z.; Wolynes, P. G. *Proc. Natl. Acad. Sci. U.S.A.* **2004**, *101*, 3352−3357.
(5) Dadarlat, V. M.; Post, C. B. *Proc. Natl. Acad. Sci. U.S.A.* **2003**, *100*, 14778−14783.
(6) Uversky, V. N.; Gillespie, J. R.; Fink, A. L. *Proteins: Struct., Funct. Bioinf.* **2000**, *41*, 415−427.
(7) Mao, A. H.; Crick, S. L.; Vitalis, A.; Chicoine, C. L.; Pappu, R. V. *Proc. Natl. Acad. Sci. U.S.A.* **2010**, *107*, 8183−8188.
(8) Khodadadi, S.; Pawlus, S.; Sokolov, A. P. *J. Phys. Chem. B* **2008**, *112*, 14273−14280.
(9) Demmel, F.; Doster, W.; Petry, W.; Schulte, A. *Eur. Biophys. J.* **1997**, *26*, 327−335.
(10) Svergun, D. I.; Richard, S.; Koch, M. H. J.; Sayers, Z.; Kuprin, S.; Zaccai, G. *Proc. Natl. Acad. Sci. U.S.A.* **1998**, *95*, 2267−2272.
(11) Levy, Y.; Onuchic, J. *Annu. Rev. Biophys. Biomol. Struct.* **2006**, *35*, 389−415.
(12) Giovambattista, N.; Lopez, C. F.; Rossky, P. J.; Debenedetti, P. G. *Proc. Natl. Acad. Sci. U.S.A.* **2008**, *105*, 2274−2279.
(13) Barlow, D. J.; Thornton, J. M. *Biopolymers* **1986**, *25*, 1717−1733.
(14) Heringa, J.; Argos, P. *J. Mol. Biol.* **1991**, *220*, 151−171.
(15) Chandler, D. *Nature* **2005**, *437*, 640−647.
(16) Abbyad, P.; Shi, X.; Childs, W.; McAnaney, T. B.; Cohen, B. E.; Boxer, S. G. *J. Phys. Chem. B* **2007**, *111*, 8269−8276.
(17) Gray, H. B.; Winkler, J. R. *Proc. Natl. Acad. Sci. U.S.A.* **2005**, *102*, 3534−3539.
(18) Born, M. *Z. Phys.* **1920**, *1*, 45−48.
(19) Onsager, L. *J. Am. Chem. Soc.* **1936**, *58*, 1486−1493.
(20) Marcus, R. A.; Sutin, N. *Biochim. Biophys. Acta* **1985**, *811*, 265−322.
(21) Hwang, J.-K.; Warshel, A. *J. Am. Chem. Soc.* **1987**, *109*, 715−720.
(22) Chaikin, P. M.; Lubensky, T. C. *Principles of condensed matter physics*; Cambridge University Press: Cambridge, UK, 1995.
(23) Fenimore, P. W.; Frauenfelder, H.; McMahon, B. H.; Young, R. D. *Proc. Natl. Acad. Sci. U.S.A.* **2004**, *101*, 14408−14413.
(24) Henzler-Wildman, K.; Kern, D. *Nature* **2007**, *450*, 964−972.
(25) Frauenfelder, H.; Chen, G.; Berendzen, J.; Fenimore, P. W.; Jansson, H.; McMahon, B. H.; Stroe, I. R.; Swenson, J.; Young, R. D. *Proc. Natl. Acad. Sci. U.S.A.* **2009**, *106*, 5129−5134.

(26) Li, T.; Hassanali, A. A.; Singer, S. J. *J. Phys. Chem. B* **2008**, *112*, 16121−16134.
(27) Matyushov, D. V. *J. Phys. Chem. B* **2011**, *115*, 10715−10724.
(28) Harpole, K. W.; Sharp, K. A. *J. Phys. Chem. B* **2011**, *115*, 9461−9472.
(29) Marlow, M. S.; Dogan, J.; Frederick, K. K.; Valentine, K. G.; Wand, A. J. *Nat. Chem. Biol.* **2010**, *6*, 352−358.
(30) Karplus, M. *Nat. Chem. Biol.* **2011**, *7*, 401−404.
(31) Mallamace, F.; Corsaro, C.; Mallamace, D.; Baglioni, P.; Stanley, H. E.; Chen, S.-H. *J. Phys. Chem. B* **2011**, *115*, 14280−14294.
(32) LeBard, D. N.; Matyushov, D. V. *Phys. Chem. Chem. Phys.* **2010**, *12*, 15335−15348.
(33) Meech, S. R. *Chem. Soc. Rev.* **2009**, *38*, 2922−2934.
(34) Tsien, R. Y. *Annu. Rev. Biochem.* **1998**, *67*, 509−544.
(35) Vallverdu, G.; Demachy, I.; Ridard, J.; Lévy, B. *J. Mol. Struct.: THEOCHEM* **2009**, *898*, 73−81.
(36) Ormö, M.; Cubitt, A. B.; Kallio, K.; Gross, L. A.; Tsien, R. Y.; Remington, S. J. *Science* **1996**, *273*, 1392−1395.
(37) Lax, M. *J. Chem. Phys.* **1952**, *20*, 1752−1760.
(38) Matyushov, D. V. *Acc. Chem. Res.* **2007**, *40*, 294−301.
(39) Marcus, R. A. *J. Phys. Chem.* **1989**, *93*, 3078−3086.
(40) Small, D. W.; Matyushov, D. V.; Voth, G. A. *J. Am. Chem. Soc.* **2003**, *125*, 7470−7478.
(41) Barbara, P. F.; Meyer, T. J.; Ratner, M. A. *J. Phys. Chem.* **1996**, *100*, 13148−13168.
(42) Matyushov, D. V.; Schmid, R.; Ladanyi, B. M. *J. Phys. Chem. B* **1997**, *101*, 1035−1050.
(43) Angell, C. A. *Science* **1995**, *267*, 1924−1935.
(44) Friesen, A. D.; Matyushov, D. V. *J. Chem. Phys.* **2011**, *135*, 104501.
(45) Zhong, D.; Pal, S. K.; Zewail, A. H. *Chem. Phys. Lett.* **2011**, *503*, 1−11.
(46) Bhattacharyya, K. *Acc. Chem. Res.* **2003**, *36*, 95.
(47) Makarov, V. A.; Andrews, B. K.; Smith, P. E.; Pettitt, B. M. *Biophys. J.* **2000**, *79*, 2966−2974.
(48) Laage, D.; Stirnemann, G.; Sterpone, F.; Rey, R.; Hynes, J. T. *Annu. Rev. Phys. Chem.* **2011**, *62*, 395−416.
(49) Nucci, N. V.; Pometun, M. S.; Wand, A. J. *J. Am. Chem. Soc.* **2011**, *133*, 12326−12329.
(50) Vitkup, D.; Ringe, D.; Petsko, G. A.; Karplus, M. *Nat. Struct. Biol.* **2000**, *7*, 34−38.
(51) Tarek, M.; Tobias, D. J. *Phys. Rev. Lett.* **2002**, *88*, 138101.
(52) Stavrov, S. S.; Solntsev, K. M.; Tolbert, L. M.; Huppert, D. *J. Am. Chem. Soc.* **2006**, *128*, 1540−1546.
(53) Khodadadi, S.; Malkovskiy, A.; Kisliuk, A.; Sokolov, A. P. *Biochim. Biophys. Acta* **2010**, *1804*, 15−19.
(54) Matyushov, D. V.; Morozov, A. Y. *Phys. Rev. E* **2011**, *84*, 011908.
(55) LeBard, D. N.; Kapko, V.; Matyushov, D. V. *J. Phys. Chem. B* **2008**, *112*, 10322−10342.
(56) Thirumalai, D.; O'Brien, E. P.; Morrison, G.; Hyeon, C. *Annu. Rev. Biophys.* **2010**, *39*, 159−183.
(57) Nicholls, D. G.; Ferguson, S. J. *Bioenergetics 3*; Academic Press: London, 2002.
(58) Tripathy, J.; Beck, W. F. *J. Phys. Chem. B* **2010**, *114*, 15958−15968.